Arch. Min. Sci. **70** (2025), 4, 675-689

Electronic version (in color) of this paper is available: http://mining.archives.pl

DOI: https://doi.org/10.24425/ams.2025.157454

MARTA SKIBA[1*], MATEUSZ KUDASIK[1], PAWEŁ BARAN[1], ANNA PAJDAK[1]

LINKING MACERAL COMPOSITION WITH STRUCTURAL AND METHANE SORPTION PROPERTIES OF BITUMINOUS COAL: AN APPROACH USING ARTIFICIAL NEURAL NETWORKS

This study investigates the structural and sorption properties of coal maceral groups from Poland. Seven fractions with varying maceral compositions were obtained by gravity separation, and their maceral proportions were determined using an automated classification method based on artificial neural networks. The samples were analyzed by microscopy, low-pressure gas adsorption, and methane adsorption and diffusion measurements. Results showed that a higher vitrinite content was associated with greater CH_4 adsorption capacity, while inertinite-rich fractions exhibited lower values. The estimated adsorption capacity of pure vitrinite reached 14.3 cm^3/g at 1.5 MPa, nearly double that of pure inertinite (6.78 cm^3/g). Diffusion analysis revealed that fractions with lower vitrinite content demonstrated significantly higher diffusion coefficients, highlighting the key role of maceral composition in methane storage and transport in coal.

Keywords: Coal; maceral groups; vitrinite; artificial neural networks; adsorption; pore structure

1. Introduction

Bituminous coal consists of a carbon matrix and functional groups, along with natural gases such as methane (CH_4), which are generated during coal metamorphism and shape its structural and adsorption properties. The coal structure is influenced by physicochemical conditions, burial depth, seam thickness, and the geological properties of overburden rocks, which together make coal a heterogeneous material with a complex pore system [1].

Coal consists of three main maceral groups: vitrinite, inertinite, and liptinite [2,3]. Vitrinite, derived from woody plant tissues, is the most abundant in bituminous coals and exhibits increasing reflectance with coalification, appearing darker than inertinite but lighter than liptinite. It is also

[1] STRATA MECHANICS RESEARCH INSTITUTE OF THE POLISH ACADEMY OF SCIENCES, 27 REYMONTA STR., 30-059 KRAKÓW, POLAND

* Corresponding author: skiba@imgpan.pl

the most brittle of the groups. Inertinite, characterized by high hardness and reflectivity, enhances the mechanical strength of coal seams. Liptinite, comprising spores, cutin, resins, waxes, and vegetable fats, has the lowest reflectivity and is distinguished by fluorescence under blue or UV light, which diminishes with coalification [4,5].

Maceral identification can be performed manually or automatically using artificial intelligence methods [6,7], or deep learning (DL) [8,9]. In the work of Iwaszenko and Róg [6], the authors used convolutional neural networks (CNNs) to segment petrographic coal images. A U-Net model was proposed for segmenting groups of macerals. Satisfactory segmentation results were obtained in the vitrinite and inertinite groups, while the liptinite group was more difficult to segment. In the work of Lei et al. [8], an improved U-Net enhanced with attention gates was used to segment maceral groups. Using the proposed method, a state-of-the-art segmentation accuracy of 91.56% was achieved. The results showed the method's great potential in automatic identification of maceral groups.

Macerals play a central role in methane formation and storage in coal [10-14]. Their composition influences pore structure and sorption properties [15-18]. Inertinite typically shows the highest porosity, followed by vitrinite and liptinite [19]. However, vitrinite-rich coals often exhibit greater methane adsorption capacity than inertinite-rich coals of similar rank [11-14,20-24]. This is linked to their higher micropore content, especially in collotelinite, whereas inertinite macerals often contain more mesopores [25]. Reactive inertinite, structurally similar to vitrinite, may further enhance methane adsorption in some coals [14].

Research on the impact of petrographic composition on coal sorption capacity has produced mixed results [26]. Many studies confirm that vitrinite-rich coals exhibit higher adsorption capacity than inertinite-dominated dull coals, due to their greater proportion of micropores [14,15,27-29]. However, some works report higher adsorption in inertinite-rich coals, particularly for fusinite varieties such as pyrofusinite and degradofusinite [30,31].

The degree of coalification also significantly affects adsorption [22,32]. Higher-rank coals generally show greater adsorption capacity due to intramolecular micropores formed during thermal degradation of organic matter [33,34]. In high-carbon coals, kerogen cracking generates methane and opens new pores, enhancing gas storage [35]. In contrast, low-rank vitrinite macerals contain more micropores than inertinite, offering more active adsorption sites, but with increasing coalification, vitrinite mesoporosity declines [36].

Petrographic composition also controls diffusion kinetics, expressed by the effective diffusion coefficient [37]. Vitrinite, rich in micropores, has high adsorption capacity but low diffusivity, while inertinite, with meso- and macropores, shows lower capacity but higher diffusivity. Desorption typically begins in meso- and macropores before being governed by micropores [13]. Studies on Polish coals confirmed that low-reflectance vitrinite samples had the highest CH_4 adsorption and diffusion coefficients, strongly influenced by temperature [38]. Overall, gas diffusion kinetics is governed by maceral composition, pore structure, and coalification degree [39-40].

Laxminarayana and Crosdale [22] and Kiani et al. [31] studied gas diffusion in Australian coals and found higher diffusion rates in inertinite-rich coals compared to vitrinite-rich ones. They also reported a negative correlation between diffusion and coal rank. Similar results were obtained by Staib et al. [41], while Karacan [42], using X-ray computed tomography, confirmed lower diffusion coefficients in vitrinite-rich lithotypes. Mastalerz et al. [43], applying infrared spectroscopy, showed that inertinite-rich coals disperse gas more efficiently than vitrinite-rich coals.

The subject of coal research is still relevant. The geopolitical situation related to the war in Ukraine makes it necessary to become independent from mineral raw material supplies. In this

situation, ensuring Poland's energy security will require the use of coal as the primary energy source for longer than originally planned [44,45]. Overall, the influence of maceral composition on coal sorption and diffusion remains ambiguous, with major differences observed between coals from different regions [34]. The aim of this study was to investigate the relationship between maceral composition and the structural and adsorption parameters of Polish bituminous coal. Fractions with varying maceral proportions were prepared by gravity separation in heavy liquids. Their composition was determined using an automated classification method based on artificial neural networks [6]. The results of maceral separation were compared with structural and adsorption parameters, allowing integration of AI-based classification with laboratory analyses. This approach enabled estimation of the adsorption capacity of "pure" macerals, representing a novel contribution of particular relevance to European coals.

2. Research methodology

The coal samples for analysis were collected from the Polish KWK "Brzeszcze" mine, located in the Upper Silesian Coal Basin. Using the dry screening method, a grain size fraction of 0.20-0.25 mm was isolated and subjected to gravity separation. Seven fractions were obtained and subsequently analyzed through: (i) technical analyses, (ii) optical microscopy, (iii) structural studies using low-pressure gas adsorption, and (iv) methane adsorption measurements combined with diffusion kinetics analysis. Based on optical microscopy results, maceral groups in each fraction were quantitatively classified using an artificial neural network method.

2.1. Coal separation and technical analyses

Gravity enrichment, also referred to as gravity separation [46,47], was carried out by exploiting density differences between coal grains and waste rock. One of the most effective approaches for separating mineral grains is heavy-liquid separation, in which the medium density is adjusted so that heavier grains sink while lighter grains float [48,49].

In this study, bromoform (density 2.89 g/cm^3) was used as the heavy liquid. Seven beakers containing heavy liquids of different densities were prepared, using xylene as a solvent. A representative coal sample was first immersed in the least dense liquid, separating into a floating fraction (lower density) and a sinking fraction (higher density). The sinking fraction, after draining, was transferred sequentially to heavier liquids of increasing density. In each case, the floating fraction was collected on a filter, washed, and dried at 378 K.

The ash content of individual maceral fractions was determined in accordance with the Polish standard PN-ISO 1171:2002 [50]. Skeletal density was measured using helium pycnometer (AccuPyc II 1340 analyzer). The skeletal volume of the sample was obtained from the volume of helium penetrating pores with diameters $\geq 2 \times 10^{-4}$ μm. Based on skeletal volume and sample mass, skeletal density values were calculated.

2.2. Identification of maceral groups using artificial neural networks

Microscopic analyses were performed on polished sections prepared from grains of individual fractions, in accordance with the PN-ISO 7404-3 [51] standard for petrographic analysis

of bituminous coal. These sections formed the basis for imaging used in artificial neural network analysis, with methodology described in detail by Młynarczuk and Skiba [6]. A ZEISS AXIOPLAN polarizing microscope with a computer-controlled XYZ mechanical stage was used, and observations were carried out in oil immersion. Images were transferred to a computer using a Nikon DS-Fi1 CCD camera (5 Mpx resolution). A magnification of 500× was applied, as required by PN-ISO 7404-3. The final image resolution was 1280×960 pixels. For each fraction, 500 images were collected, covering the entire sample surface (measuring area of about 3.2 cm^2). Image analyses were conducted in MATLAB ver. 8.5, using the Image Processing Toolbox for image processing and the Neural Network Toolbox for maceral group classification. The use of neural networks minimized observer subjectivity, ensured reproducible results, and significantly reduced measurement time compared to traditional stereological analyses.

Five groups were identified: vitrinite, inertinite, liptinite, mineral matter, and the binder embedding the coal grains. Following Młynarczuk and Skiba [6], a multilayer perceptron (MLP) with a single hidden layer was used for automatic classification. Training a multilayer perceptron is a supervised process based on a training dataset. Each case was described by a 12-element feature vector. The network output layer consisted of 5 neurons corresponding to the identified classes. The hidden layer used 12 neurons with a hyperbolic tangent activation function, and training was performed using the Levenberg-Marquardt backpropagation algorithm.

2.3. Structural characteristics

Pore space characterization was performed using the low-pressure gas adsorption (LPA) method with an ASAP 2020 analyzer operating in the pressure range of 0-0.1 MPa, based on the volumetric method. Samples were degassed under high vacuum (UHV) at 373 K for 48 hours. CO_2 was used as the adsorbate, and measurements were conducted at 273 K in the relative pressure range $0 < p/p_0 \leq 0.029$. Structural parameters were determined using Langmuir's monolayer adsorption theory and Non-Linear Density Functional Theory (NLDFT), which accounts for the fractured shape of coal pores.

2.4. CH_4 adsorption and diffusion kinetics

CH_4 adsorption studies were conducted using the gravimetric method with an Intelligent Gravimetric Analyzer IGA-001. The measurement was based on recording changes in sample mass resulting from methane adsorption. Each coal fraction was analyzed under isothermal and isobaric conditions at 313 K and pressures of 0.1 MPa, 0.3 MPa, and 1.5 MPa, with simultaneous registration of diffusion kinetics. Before measurements, the samples were degassed under UHV at 353 K for 24 hours. The analysis included adsorption capacities with respect to CH_4, parameters of Langmuir adsorption isotherms, and values of effective diffusion coefficients.

The amount of adsorbed gas was determined using the real gas equation of state (1) [38,52-54]:

$$a = \frac{V_m}{z \cdot R \cdot T} \cdot \frac{\left(m_t - m_0\right) + F_B}{m_0 \cdot M_g} \tag{1}$$

where a [cm^3/g] is the adsorption capacity, V_m [cm^3/mol] is the molar volume of CH_4 in standard conditions, z [-] is the gas compressibility coefficient, R [J/(mol·K)] is the universal gas constant,

T [K] is the temperature, m_t [g] is the instantaneous mass of the sample, m_0 [g] is the initial mass of the sample, M_g [g/mol] is the molar mass of gas, F_B [g] is the correction compensating the buoyant force.

Langmuir's adsorption isotherms were fitted to the adsorption equilibrium points, according to the formula (2) [55]:

$$a = A \cdot \frac{b \cdot p}{1 + b \cdot p} \tag{2}$$

where: A [cm^3/g] is the maximum monolayer adsorption capacity; b [MPa^{-1}] is the Langmuir adsorption equilibrium constant; p [MPa] is the pressure.

It was assumed that in small coal grains, gas transport is mainly limited to diffusion within the pore space [56]. The kinetics of CH_4 transport in coal fractions were described using the effective diffusion coefficient (D_e) [57]. The coefficient was determined based on Timofeev's Eq. (3) [58]:

$$D_e = \frac{0.3 \cdot {R_g}^2}{\pi^2 \cdot t_{1/2}} \tag{3}$$

where:

$$R_g = \frac{1}{2}\sqrt[3]{\frac{2 \cdot d_1^2 \cdot d_2^2}{d_1 + d_2}} \tag{4}$$

where: R_g [cm] is the equivalent radius of the grain; d_1, d_2 [cm] are the minimum and maximum diameter of grains; $t_{1/2}$ [s] is the half-time of the adsorption process.

3. Results

3.1. Research material characterisation

Bituminous coal was used in the study, and its basic parameters were determined: volatile matter (V^{daf} = 41%), density (ρ = 1.4 g/cm^3), and ash content (A^d = 15.5%). According to the UN-ECE International Classification of Coals [59], it is a parabituminous, medium-grade D-rank coal. Petrographic analysis showed 49.9% of vitrinite, 43.1% of inertinite, 6.3% of liptinite, and 0.7% of mineral matter.

The coal exhibited a typical porous structure. CO_2 adsorption measurements at 298 K yielded a type I isotherm with a small hysteresis loop (Fig. 1). The maximum adsorption capacity at 0.1 MPa was 13.60 cm^3/g. The specific surface area was 81.92 m^2/g (BET) and 78.64 m^2/g (Langmuir), with a micropore volume of 0.021 cm^3/g.

The adsorption capacity of coal in relation to methane was determined (Fig. 2). Gravimetric measurements produced a type I isotherm, and the Langmuir model was fitted to the equilibrium adsorption points. At 1.5 MPa, the adsorption capacity was 12.23 cm^3/g, while the total Langmuir adsorption capacity calculated from Eq. (2) was 18.05 cm^3/g.

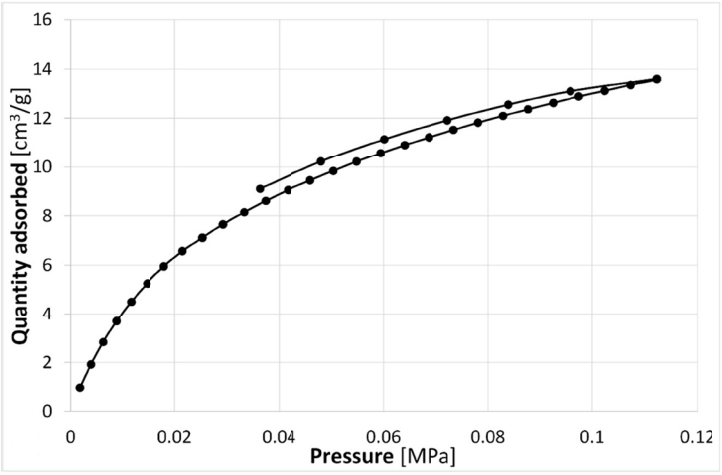

Fig. 1. Adsorption isotherms on coal in relation to carbon dioxide

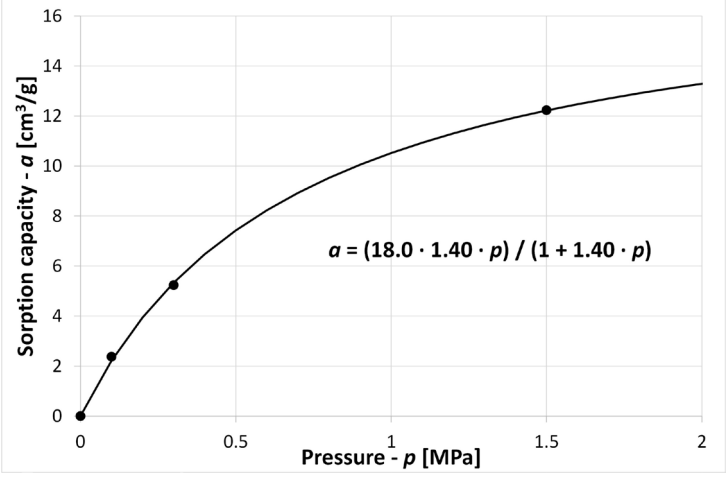

Fig. 2. CH_4 adsorption isotherms of the tested coal

As a result of gravity separation, seven fractions (N1–N7) with different densities were obtained. The N7 fraction had the highest density (1.64 g/cm^3) and ash content (33.23%).

3.2. Identification of maceral groups using artificial neural networks

Polished sections prepared from the grains of each fraction were analyzed microscopically. Representative images for the N1 and N7 fractions, characterized by contrasting technical parameters and maceral compositions, are shown in Figs. 3 and 4.

Fig. 3. Microscope images of N1 fraction (predominantly composed of vitrinite macerals, mainly collotelinite), oil immersion, magnification 500×

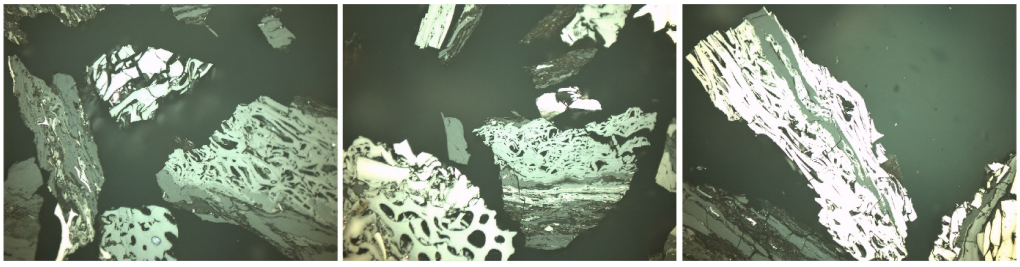

Fig. 4. Microscope images of N7 fraction (predominantly composed of inertinite macerals, mainly fusinite and semifusinite), oil immersion, magnification 500×

For each fraction, 500 images were analyzed using artificial neural networks. The resulting fractions differed in maceral composition. From N1 to N7, the vitrinite content decreased from 91.8% to 26.9%, while the inertinite content increased from 2.7% to 35.9%. Mineral matter content also increased, ranging from 1.4% to 31.7%. A strong correlation was observed between density and vitrinite content, whereas no such trend was found for inertinite content. This is confirmed by the research conducted by Jia et al. [15]. The results of automated maceral and mineral identification are summarized in TABLE 1.

TABLE 1

Results of automatic identification of maceral groups and mineral matter in coal fractions

Sample	Vitrinite content [%]	Inertinite content [%]	Liptinite content [%]	Mineral matter content [%]
N1	91.8	2.7	4.1	1.4
N2	88.2	4.2	5.5	2.1
N3	69.0	23.2	4.9	2.9
N4	47.2	40.4	5.1	7.3
N5	35.0	42.5	7.1	15.4
N6	32.0	40.5	5.2	22.3
N7	26.9	35.9	5.5	31.7

3.3. Structural analyses

Pore structure characterization was performed using low-pressure gas adsorption (LPA) at 298 K. Type I isotherms, similar to Langmuir curves, were obtained (Fig. 5a), with a good fit between experimental data and the Langmuir model ($R_L \approx 1$). A slight adsorption-desorption hysteresis was observed in several samples. The adsorption capacity relation to CO_2 correlated positively with vitrinite content, ranging from 10.30 to 20.38 cm^3/g. At 0.1 MPa, the CO_2 isotherms flattened, and the extrapolated Langmuir adsorption capacity ($p \rightarrow \infty$) was slightly higher.

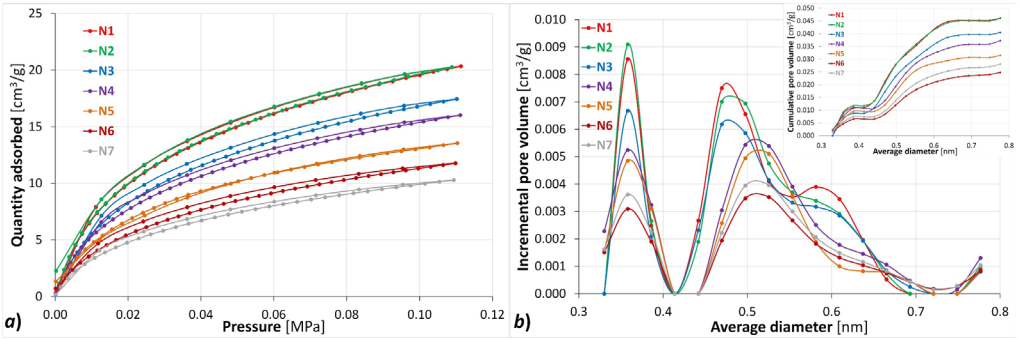

Fig. 5. LPA analysis results: a) adsorption isotherms, b) pore size distribution – NLDFT model

Maceral composition, together with coal rank and type, strongly influences pore structure [13]. In the vitrinite-rich N1 fraction, the Langmuir monolayer surface area reached 112 m^2/g. Assuming multilayer adsorption of CO_2, the BET surface area (SSA_{BET}) ranged from 55 to 107 m^2/g (TABLE 2). The vitrinite-rich fractions also showed larger pore volumes, as indicated by pore size distributions (Fig. 5b). Increased pore volumes were observed in the 0.35-0.45 nm and 0.45-0.65 nm ranges (NLDFT model).

TABLE 2

Results of structural analyses obtained by the LPA method

Sample	$a(p)$ [cm^3/g]	Q_m [cm^3/g]	SSA_L [m^2/g]	b	R_L	SSA_{BET} [m^2/g]	V_{NLDFT} [cm^3/g]
N1	20.38	24.64	112.56 ± 1.67	0.035	0.996	107.47 ± 1.39	0.046
N2	20.16	24.42	111.58 ± 1.75	0.036	0.996	106.67 ± 1.47	0.046
N3	17.47	21.73	98.53 ± 1.51	0.032	0.996	93.95 ± 1.27	0.040
N4	16.13	19.26	88.00 ± 1.57	0.035	0.994	84.03 ± 1.34	0.037
N5	13.44	16.13	73.59 ± 1.20	0.038	0.996	70.37 ± 1.02	0.032
N6	11.65	14.34	66.02 ± 1.33	0.032	0.993	62.94 ± 1.14	0.028
N7	10.30	12.54	57.81 ± 1.25	0.032	0.993	55.12 ± 1.06	0.025

where: $a(p)$ is the adsorption capacity at 0.1 MPa; Q_m is the total adsorption capacity at $p \rightarrow \infty$; SSA_L, SSA_{BET} are the specific surface area according to Langmuir and BET model; b is the coefficient in Langmuir model; R_L is the correlation coefficient in Langmuir model; V_{NLDFT} is the total pore volume according to NLDFT theory.

3.4. Studies of CH_4 adsorption and diffusion kinetics

Methane adsorption was studied using the gravimetric method. Langmuir adsorption isotherms were fitted to equilibrium data by the least-squares method, producing type I isotherms. CH_4 adsorption capacity varied with pressure and maceral composition (Fig. 6). The highest capacities were recorded in vitrinite-rich, inertinite-poor fractions.

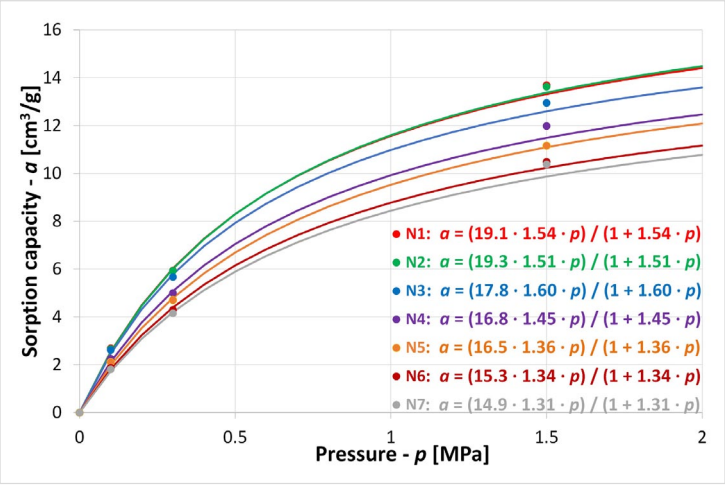

Fig. 6. CH_4 adsorption isotherms of the tested coal fractions

To analyze the effect of petrographic composition on adsorption properties, the relationships between maceral and mineral content and CH_4 adsorption capacity were determined (Fig. 7). Langmuir constants b (from Eq. (2)) ranged from 1.31 to 1.54 MPa^{-1}, with the highest values in vitrinite-rich fractions and decreasing values with increasing inertinite content. This indicates stronger CH_4 binding in vitrinite than in inertinite. Vitrinite content showed a positive correlation with CH_4 adsorption (Fig. 7a), whereas inertinite, liptinite, and mineral matter were negatively correlated (Figs. 7b-d).

Linear relationships describing the dependence of CH_4 adsorption on maceral and mineral contents enabled estimation of the adsorption capacities of "pure" components (TABLE 3).

TABLE 3

Estimated adsorption capacities to CH_4 of "pure" maceral groups and mineral matter

	Adsorption capacity of "pure" macerals [cm^3/g]			
Pressure [MPa]	**Vitrinite**	**Inertinite**	**Liptinite**	**Mineral matter**
0.1	2.86	0.96	0	0
0.3	6.29	2.32	0	0
1.5	14.30	6.78	0	2.17
$p \rightarrow \infty$	20.60	11.84	0	6.75

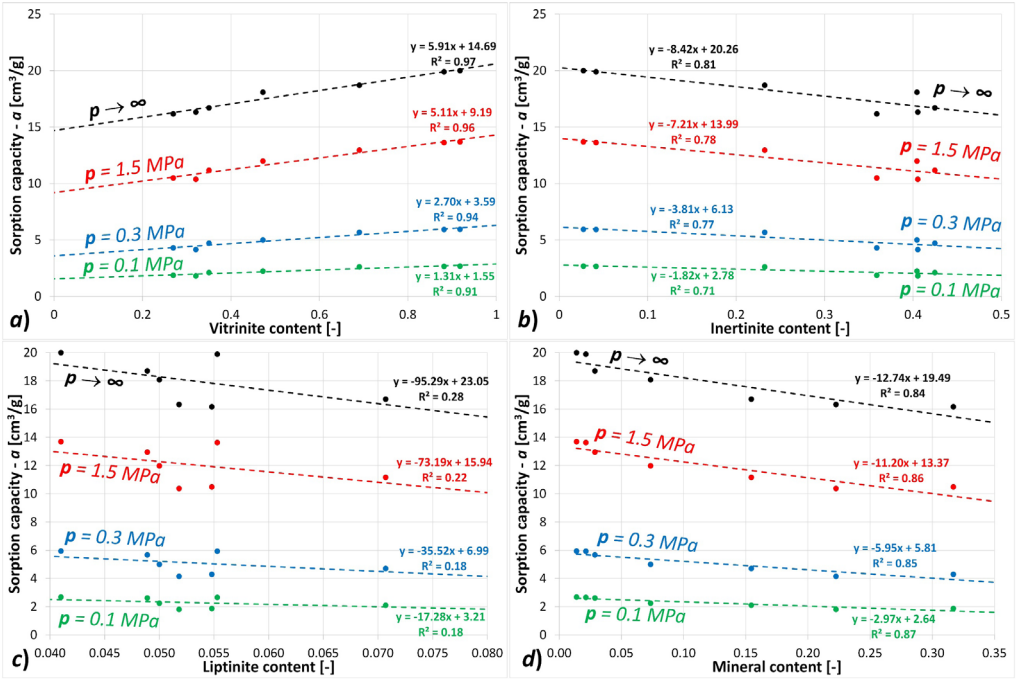

Fig. 7. The influence of the relative content of macerals and mineral matter content on the adsorption capacity in relation to CH_4

Vitrinite exhibited the highest CH_4 adsorption capacity, approximately twice that of inertinite. Liptinite showed negligible CH_4 adsorption, while mineral matter contributed minimally at higher pressures. However, due to the low liptinite content (<8%), the estimated CH_4 adsorption for a "pure" liptinite sample (100%) is subject to high uncertainty, as reflected in the low coefficient of determination (R^2). For vitrinite, a strong linear correlation was obtained ($R^2 > 0.9$) in the 0.2-0.9 composition range.

The influence of maceral composition on CH_4 diffusion kinetics was also investigated. Effective diffusion coefficients (D_e) were calculated using Eq. (3), based on CH_4 adsorption curves at 0.1 MPa. D_e values ranged from 1.01×10^{-9} to 9.36×10^{-9} cm^2/s and were strongly dependent on maceral composition. A negative correlation was observed between vitrinite content and D_e values, described by an exponential function (Fig. 8). The D_e of the vitrinite-poor N7 fraction was nearly an order of magnitude higher than that of the vitrinite-rich N1 fraction.

4. Discussion and conclusions

The study investigated the relationship between maceral composition and the structural and adsorption properties of Polish bituminous coal. Seven density-separated fractions were analyzed, each characterized by different proportions of vitrinite, inertinite, liptinite, and mineral matter. The maceral composition of individual fractions was identified using a proprietary classifica-

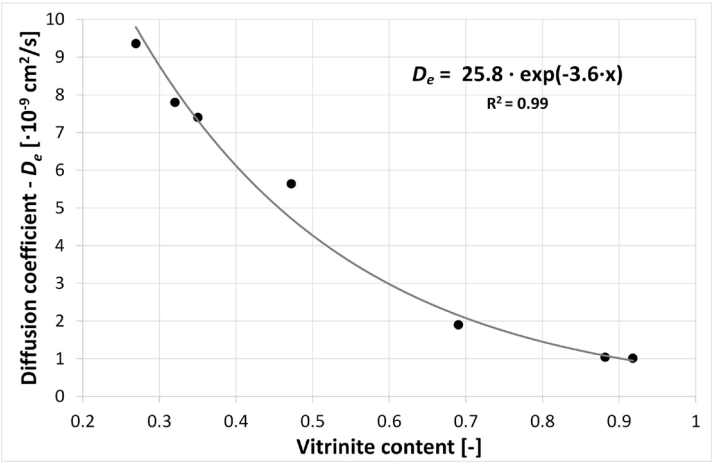

Fig. 8. Dependence of the value of the effective diffusion coefficient on the vitrinite content of coal

tion method based on a multilayer perceptron neural network, which ensured high accuracy and repeatability of maceral group identification.

Structural and adsorption analyses revealed distinct differences between the fractions. The BET specific surface area and micropore volume were positively correlated with vitrinite content. In vitrinite-rich fractions, SSA_{BET} reached 107.5 m^2/g and micropore volume 0.05 cm^3/g, while in inertinite-rich fractions, these values were significantly lower (55.1 m^2/g and 0.02 cm^3/g, respectively). The pores were mainly concentrated in the 3.5-4.0 nm and 4.5-6.5 nm ranges. These results confirm earlier findings that the pore structure of coal depends strongly on its maceral composition and rank [13,60]. Similar relationships were reported for coals from India [61] and China [15,62], where vitrinite was also found to dominate micropore development. However, Shan et al. [63] observed the opposite trend, with the highest surface areas in inertinite-rich coals, highlighting that local geological conditions may also play a role.

Methane adsorption studies showed that the CH_4 adsorption capacity increased with vitrinite content and decreased with increasing inertinite, liptinite, and mineral matter contents. The highest adsorption capacity was observed in vitrinite-rich fractions (a = 14.3 cm^3/g at 1.5 MPa), approximately twice that of inertinite (a = 6.78 cm^3/g). Liptinite did not exhibit measurable adsorption, while mineral matter contributed slightly at higher pressures. The diffusion coefficient (D_e) also depended on maceral composition: in the vitrinite-rich N1 fraction (Vt = 91.8%), $D_e = 1.01\times10^{-9}$ cm^2/s, whereas in the vitrinite-poor N7 fraction (Vt = 26.9%), $D_e = 9.36\times10^{-9}$ cm^2/s. These results confirm that while vitrinite increases adsorption capacity, it also slows diffusion kinetics due to its highly microporous structure. Similar conclusions were drawn by Laxminarayana and Crosdale [22], Staib et al. [41], and Karacan [42]. The observed relationships are consistent with studies of coals from North America and other regions [34, 64-67], where methane adsorption was found to depend mainly on the microporous structure. However, Kiani et al. [31] reported that in Australian bituminous coals, maceral composition affected porosity and adsorption kinetics rather than the total adsorption capacity, indicating regional variability. The role of vitrinite as the main microporous and adsorption-active maceral is therefore confirmed, although the magnitude of its effect may vary with coal type, rank, and moisture content [33,68].

Methane is primarily stored in coal by adsorption onto micropore surfaces. Consequently, the pore surface area is a critical factor determining coal's gas-bearing potential [67]. Vitrinite, being rich in micropores, contributes most to methane adsorption [23]. In contrast, in liptinite-rich coals, methane is retained in pores as a dissolved gas rather than adsorbed on their surfaces [14], explaining the weak correlation between structure and adsorption capacity in such coals.

The presented results demonstrate a clear coupling between maceral composition, microporous structure, and gas adsorption–diffusion behavior. Vitrinite enhances CH_4 storage capacity but reduces diffusion kinetics, while inertinite contributes to faster gas transport with lower adsorption potential. Liptinite and minerals play only a minor role in methane accumulation. The determination of the adsorption capacity of "pure" maceral groups provides a valuable quantitative insight into their intrinsic properties, previously only qualitatively discussed.

The applied methodology combining heavy-liquid separation with neural network based maceral identification represents a novel approach to coal characterization. It enables a more precise assessment of the contribution of specific maceral groups to gas storage and transport phenomena. The findings not only expand the understanding of the microstructural controls on adsorption processes in European coals but also have practical implications for predicting gas content and migration potential in coal seams.

Overall, the results demonstrate that vitrinite is the dominant maceral controlling methane adsorption and pore development in bituminous coal. Its high microporosity enhances methane adsorption capacity but simultaneously reduces diffusion rates. Inertinite, by contrast, contributes to faster gas transport but exhibits lower adsorption potential, while liptinite and mineral matter play only a minor role in methane accumulation. The structural and adsorption characteristics observed in Polish coals are consistent with global findings, although regional geological conditions may modify the strength of these relationships. The application of neural network based maceral identification, combined with heavy liquid separation, has proven to be an effective and innovative method for distinguishing the contributions of individual maceral groups to gas storage and transport processes in coal seams. These findings significantly enhance the understanding of the petrological and structural factors governing gas storage and migration in coal, with practical implications for both coalbed methane recovery and CO_2 sequestration.

Acknowledgments

The authors would like to thank Mirosław Wierzbicki, PhD, for his support of the research idea and Jarosław Aksamit for technical assistance.
The work was conducted in Strata Mechanics Research Institute of The Polish Academy of Sciences and it was supported by the Ministry of Science and Higher Education

References

[1] J. Rouquerol, D. Avnir, C.W. Fairbridge, D.H. Everett, J.M. Haynes, N. Pernicone, J.D.F. Ramsay, K.S.W. Sing, K.K. Unger, Recommendations for the characterization of porous solids (Technical Report), 1739-1758 (1994). DOI: https://doi.org/10.1351/pac199466081739

[2] The new inertinite classification (ICCP System 1994). Fuel **80** (4), 459-471 (2001). DOI: https://doi.org/10.1016/S0016-2361(00)00102-2

[3] The new vitrinite classification (ICCP System 1994),. Fuel **77** (5), 349-358 (1998). DOI: https://doi.org/10.1016/S0016-2361(98)80024-0

[4] E. Stach, Stach's Textbook of Coal Petrology. Schweizerbart Science Publishers, Stuttgart, Germany (1982).

[5] C.F.K. Diessel, Coal_Bearing_Depositional_Systems. Springer-Verlag, Ed. (1982). DOI: https://doi.org/10.1007/978-3-642-75668-9

[6] M. Mlynarczuk, M. Skiba, The application of artificial intelligence for the identification of the maceral groups and mineral components of coal. Comput Geosci **103**, 133-141 (2017). DOI: https://doi.org/10.1016/j.cageo.2017.03.011

[7] M. Skiba, The influence of the discrepancies in the observers' decisions on the process of identification of maceral groups using artificial neural networks. Journal of Sustainable Mining **15** (4), 151-155 (2016). DOI: https://doi.org/10.1016/j.jsm.2017.03.001

[8] M. Lei, Z. Rao, H. Wang, Y. Chen, L. Zou, H. Yu, Maceral groups analysis of coal based on semantic segmentation of photomicrographs via the improved U-net. Fuel **294**, 120475 (2021). DOI: https://doi.org/10.1016/j.fuel.2021.120475

[9] S. Iwaszenko, L. Róg, Application of Deep Learning in Petrographic Coal Images Segmentation. Minerals **11** (11) (2021). DOI: https://doi.org/10.3390/min11111265

[10] J. Kumar, V.A. Mendhe, A.D. Kamble, M. Bannerjee, S. Mishra, B.D. Singh, V.K. Mishra, P.K. Singh, H. Singh, Coalbed methane reservoir characteristics of coal seams of south Karanpura coalfield, Jharkhand, India. Int. J. Coal Geol. **196**, 185-200 (2018). DOI: https://doi.org/10.1016/j.coal.2018.07.011

[11] S.M. Mardon, C.F. Eble, J.C. Hower, K. Takacs, M. Mastalerz, R. Marc Bustin, Organic petrology, geochemistry, gas content and gas composition of Middle Pennsylvanian age coal beds in the Eastern Interior (Illinois) Basin: Implications for CBM development and carbon sequestration. Int. J. Coal Geol. **127**, 56-74 (2014). DOI: https://doi.org/10.1016/j.coal.2014.02.002

[12] M.N. Lamberson, R.M. Bustin, Coalbed methane characteristics of Gates Formation coals, northeastern British Columbia: Effect of maceral composition. Am. Assoc. Pet. Geol. Bull. **77** (12), United States (1993).

[13] P.J. Crosdale, B.B. Beamish, M. Valix, Coalbed methane sorption related to coal composition. Int. J. Coal Geol. **35** (1-4), 147-158 (1998). DOI: https://doi.org/10.1016/S0166-5162(97)00015-3

[14] G.R.L. Chalmers, R. Marc Bustin, On the effects of petrographic composition on coalbed methane sorption. Int. J. Coal Geol. **69** (4), 288-304 (2007). DOI: https://doi.org/10.1016/j.coal.2006.06.002

[15] T. Jia, S. Zhang, S. Tang, D. Xin, Q. Zhang, K. Zhang, Pore Structure and Adsorption Characteristics of Maceral Groups: Insights from Centrifugal Flotation Experiment of Coals. ACS Omega **8** (13), 12079-12097, American Chemical Society (2023). DOI: https://doi.org/10.1021/acsomega.2c07876

[16] M. Bukowska, U. Saneta, M. Wadas, Zonation of deposits of hard coals of different porosity in the Upper Silesian Coal Basin. Gospodarka Surowcami Mineralnymi – Mineral Resources Management **32** (1), 5-24, Komitet Zrównoważonej Gospodarki Surowcami Mineralnymi Polska Akademia Nauk (2016). DOI: https://doi.org/10.1515/gospo-2016-0009

[17] B. Bielowicz, Change of the petrographic composition of lignite during the ex-situ lignite gasification. Fuel **206**, 219-229 (2017). DOI: https://doi.org/10.1016/j.fuel.2017.06.006

[18] A. Dudzińska, J. Cygankiewicz, M. Włodarek, Natural content of gases: Carbon monoxide, carbon dioxide, hydrogen and unsaturated hydrocarbons of ethylene, propylene and acetylene in selected bituminous coal seams. Int. J. Coal Geol. **178**, 110-121 (2017). DOI: https://doi.org/10.1016/j.coal.2017.05.005

[19] D.W. van Krevelen, J. Schuyler, Coal Science: Aspects of Coal Constitution. 1st ed., Elsevier Publishing Company, Amsterdam (1957).

[20] C.R. Clarkson, R.M. Bustin, The effect of pore structure and gas pressure upon the transport properties of coal: a laboratory and modeling study. 1. Isotherms and pore volume distributions. Fuel **78** (11), 1333-1344 (1999). DOI: https://doi.org/10.1016/S0016-2361(99)00055-1

[21] C.R. Clarkson, R.M. Bustin, Variation in permeability with lithotype and maceral composition of Cretaceous coals of the Canadian Cordillera. Int. J. Coal Geol. **33** (2), 135-151, Elsevier (1997). DOI: https://doi.org/10.1016/S0166-5162(96)00023-7

[22] C. Laxminarayana, P.J. Crosdale, Role of coal type and rank on methane sorption characteristics of Bowen Basin, Australia coals. Int. J. Coal Geol. **40** (4), 309-325 (1999). DOI: https://doi.org/10.1016/S0166-5162(99)00005-1

[23] M. Mastalerz, H. Gluskoter, J. Rupp, Carbon dioxide and methane sorption in high volatile bituminous coals from Indiana, USA. Int. J. Coal Geol. **60** (1), 43-55 (2004). DOI: https://doi.org/10.1016/j.coal.2004.04.001

[24] A. Hildenbrand, B.M. Krooss, A. Busch, R. Gaschnitz, Evolution of methane sorption capacity of coal seams as a function of burial history – a case study from the Campine Basin, NE Belgium. Int. J. Coal Geol. **66** (3), 179-203 (2006). DOI: https://doi.org/10.1016/j.coal.2005.07.006

[25] M. Mastalerz, A. Drobniak, D. Strąpoć, W. Solano Acosta, J. Rupp, Variations in pore characteristics in high volatile bituminous coals: Implications for coal bed gas content. Int. J. Coal Geol. **76** (3), 205-216 (2008). DOI: https://doi.org/10.1016/j.coal.2008.07.006

[26] A. Olajossy, On The Effects Of Maceral Content On Methane Sorption Capacity In Coals. Archives of Mining Sciences **4**, (2013). DOI: https://doi.org/10.2478/amsc-2013-0083

[27] Z. Weishauptová, O. Přibyl, I. Sýkorová, V. Machovič, Effect of bituminous coal properties on carbon dioxide and methane high pressure sorption. Fuel **139**, 115-124 (2015). DOI: https://doi.org/10.1016/j.fuel.2014.08.030

[28] P. Dutta, S. Bhowmik, S. Das, Methane and carbon dioxide sorption on a set of coals from India. Int. J. Coal Geol. **85** (3), 289-299 (2011). DOI: https://doi.org/10.1016/j.coal.2010.12.004

[29] R. Walker, M. Glikson, M. Mastalerz, Relations between coal petrology and gas content in the Upper Newlands Seam, central Queensland, Australia. Int. J. Coal Geol. **46** (2), 83-92 (2001). DOI: https://doi.org/10.1016/S0166-5162(01)00015-5

[30] Ettinger, I. Eremin, B. Zimakov, M. Yanovskaya, Natural factors influencing coal sorption properties. I. Petrography and sorption properties of coals. Fuel **45** (4), 267-275 (1966).

[31] A. Kiani, R. Sakurovs, M. Grigore, A. Sokolova, Gas sorption capacity, gas sorption rates and nanoporosity in coals. Int. J. Coal Geol. **200**, 77-86 (2018). DOI: https://doi.org/10.1016/j.coal.2018.10.012

[32] P. Waszczuk-Zellner, M. Lutyński, A. Koteras, Factors Influencing Potential CO2 Storage Capacity in Shales. Archives of Mining Sciences **67** (1), 143-157 (2022). DOI: https://doi.org/10.24425/ams.2022.140707

[33] J.H. Levy, S.J. Day, J.S. Killingley, Methane capacities of Bowen Basin coals related to coal properties. Fuel **76** (9), 813-819 (1997). DOI: https://doi.org/10.1016/S0016-2361(97)00078-1

[34] R.M. Bustin, C.R. Clarkson, Geological controls on coalbed methane reservoir capacity and gas content. Int. J. Coal Geol. **38** (1), 3-26 (1998). DOI: https://doi.org/10.1016/S0166-5162(98)00030-5

[35] R. Scott, Hydrogeologic factors affecting gas content distribution in coal beds. Int. J. Coal Geol. **50** (1), 363-387 (2002). DOI: https://doi.org/10.1016/S0166-5162(02)00135-0

[36] J.F. Unsworth, C.S. Fowler, L.F. Jones, Moisture in coal: 2. Maceral effects on pore structure. Fuel **68** (1), 18-26 (1989). DOI: https://doi.org/10.1016/0016-2361(89)90005-7

[37] C. Laxminarayana, P.J. Crosdale, Controls on Methane Sorption Capacity of Indian Coals. Am. Assoc. Pet. Geol. Bull. **86** (2), 201-202 (2002).

[38] N. Skoczylas, A. Pajdak, M. Kudasik, L.T. Palla Braga, CH4 and CO2 sorption and diffusion carried out in various temperatures on hard coal samples of various degrees of coalification. J. Nat. Gas. Sci. Eng. **81**, 103449 (2020). DOI: https://doi.org/10.1016/j.jngse.2020.103449

[39] R. Keshavarz, R. Sakurovs, M. Grigore, M. Sayyafzadeh, Effect of maceral composition and coal rank on gas diffusion in Australian coals. Int. J. Coal Geol. **173**, 65-75, (2017). DOI: https://doi.org/10.1016/j.coal.2017.02.005

[40] M. Skiba, M. Młynarczuk, Estimation of Coal's Sorption Parameters Using Artificial Neural Networks. Materials **13** (23) (2020). DOI: https://doi.org/10.3390/ma13235422

[41] G. Staib, R. Sakurovs, E.M.A. Gray, A pressure and concentration dependence of CO2 diffusion in two Australian bituminous coals. Int. J. Coal Geol. **116-117** (2013). DOI: https://doi.org/10.1016/j.coal.2013.07.005

[42] C.Ö. Karacan, Heterogeneous Sorption and Swelling in a Confined and Stressed Coal during CO_2 Injection. Energy & Fuels **17** (6), 1595-1608 (2003). DOI: https://doi.org/10.1021/ef0301349

[43] M. Mastalerz, A. Schimmelmann, G.P. Lis, A. Drobniak, A. Stankiewicz, Influence of maceral composition on geochemical characteristics of immature shale kerogen: Insight from density fraction analysis. Int. J. Coal Geol. **103**, 60-69 (2012). DOI: https://doi.org/10.1016/j.coal.2012.07.011

[44] P. Strzałkowski, M. Maruszczyk, Hard Coal as a Necessary Energy Resource in Poland. Archives of Mining Sciences **69**, 1, 67-76 (2024). DOI: https://doi.org/10.24425/ams.2024.149827

[45] S. Tokarski, A. Tajduś, National Energy and Climate Plan: How Much Coal for the Polish Energy Sector by 2040? Archives of Mining Sciences **70** (2), 313-330 (2025). DOI: https://doi.org/10.24425/ams.2025.154665

[46] J. Drzymała, Podstawy mineralurgii. Wyd. 2. zmienione, Oficyna Wydawnicza Politechniki Wrocławskiej, Wrocław (2009).

[47] J. Blaschke, Procesy technologiczne w przeróbce kopalin użytecznych. Skrypt AGH 1008, AGH, Kraków (1987).

[48] T. Laskowski, S. Błaszczyński, M. Ślusarek, Wzbogacanie kopalin w cieczach ciężkich. Wydawnictwo Śląsk, Katowice (1979).

[49] W. Budryk, Przeróbka mechaniczna użytecznych ciał kopalnych. Akademia Górnicza, Kraków (1944).

[50] PN-ISO 1171:2002: Paliwa stałe – Oznaczanie popiołu. Polski Komitet Normalizacyjny, Warszawa (2002).

[51] PN-ISO 7404-3, 2001: Metody analizy petrograficznej węgla kamiennego (bitumicznego) i antracytu. Polski Komitet Normalizacyjny, Warszawa (2001).

[52] M. Kudasik, The manometric sorptomat – an innovative volumetric instrument for sorption measurements performed under isobaric conditions. Meas. Sci. Technol. **27** (3), 035903 (2016). DOI: https://doi.org/10.1088/0957-0233/27/3/035903

[53] M. Kudasik, Results of comparative sorption studies of the coal-methane system carried out by means of an original volumetric device and a reference gravimetric instrument, Adsorption **23**(4), 613–626 (2017). DOI: 10.1007/s10450-017-9881-6

[54] M. Kudasik, N. Skoczylas, A. Pajdak, The Repeatability of Sorption Processes Occurring in the Coal-Methane System during Multiple Measurement Series. Energies (Basel) **10** (5), 4013-4033 (2017).

[55] I. Langmuir, The adsorption of gases on plane surfaces of glass, mica and platinum. J. Am. Chem. Soc. **40** (9), 1361-1403, American Chemical Society (1918).

[56] M. Gawor, N. Skoczylas, Sorption Rate of Carbon Dioxide on Coal. Transp. Porous. Media **101** (2), 269-279 (2014). DOI: https://doi.org/10.1007/s11242-013-0244-9

[57] S. Chattaraj, D. Mohanty, T. Kumar, G. Halder, Thermodynamics, kinetics and modeling of sorption behaviour of coalbed methane – A review. Journal of Unconventional Oil and Gas Resources **16**, 14-33 (2016). DOI: https://doi.org/10.1016/j.juogr.2016.09.001

[58] D.P. Timofiejew, Adsorptionkinetik. Lipsk VEB (1967).

[59] UN–ECE, 1998 – International al classification of in-seam coals. ENERGY/1998/19, United Nations, Geneva and New York (1988).

[60] W. Pickel, J. Kus, D. Flores, S. Kalaitzidis, K. Christanis, B.J. Cardott, M. Misz-Kennan, S. Rodrigues, A. Hentschel, M. Hamor-Vido, P. Crosdale, N. Wagner, Classification of liptinite – ICCP System 1994. Int. J. Coal Geol. **169**, 40-61 (2017). DOI: https://doi.org/10.1016/j.coal.2016.11.004

[61] D.P. Mishra, S.K. Verma, R.M. Bhattacharjee, R. Upadhyay, P. Sahu, Geological and microstructural characterisation of coal seams for methane drainage from underground coal mines. Bulletin of Engineering Geology and the Environment **82** (9), 341 (2023). DOI: https://doi.org/10.1007/s10064-023-03352-8

[62] M. Zhang, X. Fu, Characterization of pore structure and its impact on methane adsorption capacity for semi-anthracite in Shizhuangnan Block, Qinshui Basin. J. Nat. Gas. Sci. Eng. **60**, 49-62 (2018). DOI: https://doi.org/10.1016/j.jngse.2018.10.001

[63] C. Shan, T. Zhang, X. Liang, R. Hu, W. Zhao, Nanopore structure characteristics of high-rank vitrinite- and inertinite-coal. Acta Petrolei Sinica **41** (6), 723-736 (2020).

[64] C.I. Butland, T.A. Moore, Secondary biogenic coal seam gas reservoirs in New Zealand: A preliminary assessment of gas contents. Int. J. Coal Geol. **76** (1), 151-165 (2008). DOI: https://doi.org/10.1016/j.coal.2008.05.017

[65] M. Faiz et al., The influence of petrological properties and burial history on coal seam methane reservoir characterisation, Sydney Basin, Australia. Int. J. Coal Geol. **70** (1), 193-208 (2007). DOI: https://doi.org/10.1016/j.coal.2006.02.012

[66] P.D. Warwick, F.C. Breland, P.C. Hackley, Biogenic origin of coalbed gas in the northern Gulf of Mexico Coastal Plain, U.S.A. Int. J. Coal Geol. **76** (1), 119-137 (2008). DOI: https://doi.org/10.1016/j.coal.2008.05.009

[67] T.A. Moore, Coalbed methane: A review. Int. J. Coal Geol. **101**, 36-81 (2012). DOI: https://doi.org/10.1016/j.coal.2012.05.011

[68] A. Pajdak, Studies on the influence of moisture on the sorption and structural properties of hard coals. International Journal of Greenhouse Gas Control **103**, 103193 (2020). DOI: https://doi.org/10.1016/j.ijggc.2020.103193